Inorg. Chem. **2009**, *48*, 4362−4371

Inorganic Chemistry
Article

R_5Pn_3-type Phases of the Heavier Trivalent Rare-Earth-Metal Pnictides (Pn = Sb, Bi): New Phase Transitions for Er_5Sb_3 and Tm_5Sb_3

Shalabh Gupta, E. Alejandro León-Escamilla, Fei Wang, Gordon J. Miller, and John D. Corbett*

Ames Laboratory−DOE, and Department of Chemistry, Iowa State University, Ames, Iowa 50011

Received December 31, 2008

The syntheses and distributions of binary R_5Pn_3 phases among the hexagonal Mn_5Si_3 (*M*), and the very similar orthorhombic β-Yb_5Sb_3 (*Y*) and Y_5Bi_3 (*YB*) structure types have been studied for R = Y, Gd−Lu and Pn = Sb, Bi. Literature reports of *M* and *YB*-type structure distributions among R_5Pn_3 phases, R = Y, Gd−Ho, are generally confirmed. The reported *M*-type Er_5Sb_3 could not be reproduced. Alternate stabilization of *Y*-type structures by interstitials H or F has been disproved for these nominally trivalent metal pnictides. Single crystal structures are reported for (a) the low temperature *YB* form of Er_5Sb_3 (*Pnma*, $a = 7.9646(9)$ Å, $b = 9.176(1)$ Å, $c = 11.662(1)$ Å), (b) the *YB*- and high temperature *Y*-types of Tm_5Sb_3 (both *Pnma*, $a = 7.9262(5)$, $11.6034(5)$ Å, $b = 9.1375(6)$, $9.1077(4)$ Å, $c = 11.6013(7)$, $7.9841(4)$ Å, respectively), and (c) the *YB* structure of Lu_5Sb_3, $a = 7.8847(4)$ Å, $b = 9.0770(5)$ Å, $c = 11.5055(6)$ Å. Reversible, temperature-driven phase transitions (β-$Yb_5Sb_3 \leftrightarrows Y_5Bi_3$ types) for the former Er_5Sb_3 and Tm_5Sb_3 around 1100 °C and the means of quenching the high temperature *Y* form, have been esstablished. According to their magnetic susceptibilities, *YB*-types of Er_5Sb_3 and Tm_5Sb_3 contain trivalent cations. Tight-binding linear muffin-tin-orbital method within the atomic sphere approximation (TB-LMTO-ASA) calculations for the two structures of Tm_5Sb_3 reveal generally similar electronic structures but with subtle Tm−Tm differences supporting their relative stabilities. The ambient temperature *YB*-Tm_5Sb_3 shows a deep pseudogap at E_F, approaching that of a closed shell electronic state. Short R−R bonds (3.25−3.29 Å) contribute markedly to the structural stabilities of both types. The *Y*-type structure of Tm_5Sb_3 shows both close structural parallels to, and bonding contrasts with, the nominally isotypic, stuffed Ca_5Bi_3D and its analogues. Some contradictions in the literature are discussed.

Introduction

All of the rare-earth metal-rich pnictides R_5Pn_3 (Pn = Sb, Bi) have been reported in one or more of three common structure types: (a) the hexagonal Mn_5Si_3-type (*M*); (b) the orthorhombic β-Yb_5Sb_3-type (*Y*); or (c) the orthorhombic Y_5Bi_3-type (*YB*), all of which are metal-rich and lack Pn−Pn bonding. Although the ubiquitous Mn_5Si_3-type occurs for a wide variety of both R and Pn elements,[1,2] we shall not concern ourselves with these details. The very similar structures of interest are Y_5Bi_3[3] and β-Yb_5Sb_3[4] types, both of which occur in the same space group and setting, *Pnma,* but with reversed order of the axial lengths, $c > b > a$ versus $a > b > c$, respectively. These strikingly similar structures feature distorted hexagonal rings built from edge-sharing, Pn-centered R_6(Sb,Bi) trigonal prisms when viewed along the common *b* direction. These are illustrated in Figure 1, with the *a* and *c* directions for one reversed so as to give parallel length scales. Interest in these two structure types increased, and possible reasons for their differentiation became apparent, after the β-Yb_5Sb_3 parent and all eight isotypic Sb and Bi examples with divalent cations were shown in 1998 to be the ternary phases stabilized by a hitherto unrecognized interstitial impurity in a tetrahedral cavity.[5,6] This unrecognized interstitial, commonly hydrogen, had earlier led to numerous, troubling examples of low and

* Corresponding author. E-mail: jdc@ameslab.gov.

(1) Villars, P.; Calvert, L. D. *Pearson's Handbook of Crystallographic Data for Intermetallic Phases*, 2nd ed.; American Society for Metals International: Metals Park, OH, 1991.
(2) Leon-Escamilla, A. E.; Corbett, J. D. *Chem. Mater.* **2006**, *18*, 4782.
(3) Wang, Y.; Gabe, E. J.; Calvert, L. D.; Taylor, J. B. *Acta Crystallogr.* **1976**, *B32*, 1440.
(4) Brunton, G. D.; Steinfink, H. *Inorg. Chem.* **1971**, *10*, 2301.
(5) Leon-Escamilla, A. E.; Corbett, J. D. *J. Alloys Compd.* **1998**, *265*, 104.
(6) Leon-Escamilla, A. E.; Corbett, J. D.; Garcia, E.; Guloy, A. M.; Hurng, W.-M.; Kwon, Y.-Uk. *Chem. Mater.* **1998**, *10*, 2824.

10.1021/ic802464u CCC: $40.75

Published on Web 04/02/2009

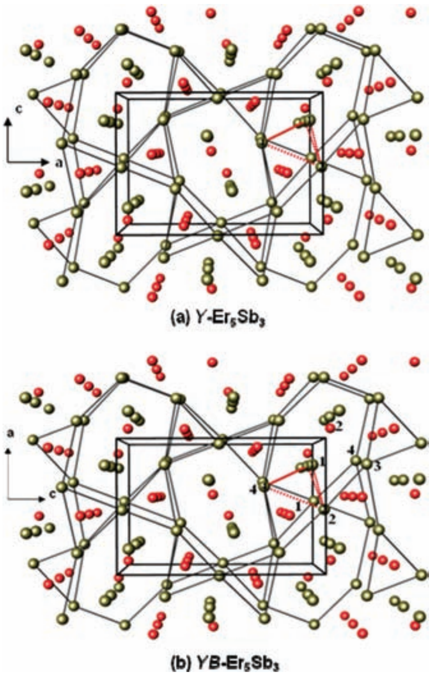

Figure 1. [010] perspective of the (a) β-Yb_5Sb_3 (*Y*) and [0$\bar{1}$0] view of the (b) Y_5Bi_3 (*YB*) type structures of Er_5Sb_3 and Tm_5Sb_3. Note the great similarities when one set of *a* and *c* axes is reversed. Olive spheres represent Er and red, Sb. Examples of the tightly bound metal tetrahedron in each are dotted. (Atoms of each type are numbered in (b).)

unpredictable yields of, and variable lattice dimensions for, supposedly binary compounds. The similarly sized fluoride substitutes well for hydride in this structure type, which allowed the first reliable X-ray structure determination for Ca_5Sb_3F (*F*- or stuffed *Y*-type).[5,7] The very similar *Y*- and *YB*-type structures can be readily distinguished by characteristic differences in their powder diffraction patterns, particularly for reflections with large *h* or *l* indices. (A comparison is shown in Figure S1, Supporting Information.) The essential role of hydrogen is easily established by the decomposition that ensues when either the reactants or the ternary product is sealed in a Nb or Ta container and heated under high vacuum to ca. 550−600 °C or higher for a few hours,[5] under which conditions Ta and Nb function as semipermeable membranes for dissociated H_2.[8] Indeed, the sealed fused silica jackets that usually enclose the metal containers during static high temperature reactions can afford appreciable hydrogen via desorbed water.

A reasonable (and unpublished) basis for the binding of H or F atoms only in the *Y*-type structures of $A^{II}_5Pn_3$ is shown in Figure 2, [100] and [001] projections of the two structure types in Figure 1. Characteristic puckering of the horizontal (020) layers only in the *Y* structure (top) helps define the characteristic columns of yellow/green tetrahedra that bind H or F atoms in the isotypic *F*-type structure. (This is an extension of a relationship noted by Wang et al. in the original report of the Y_5Bi_3 structure.[3]) In contrast, no

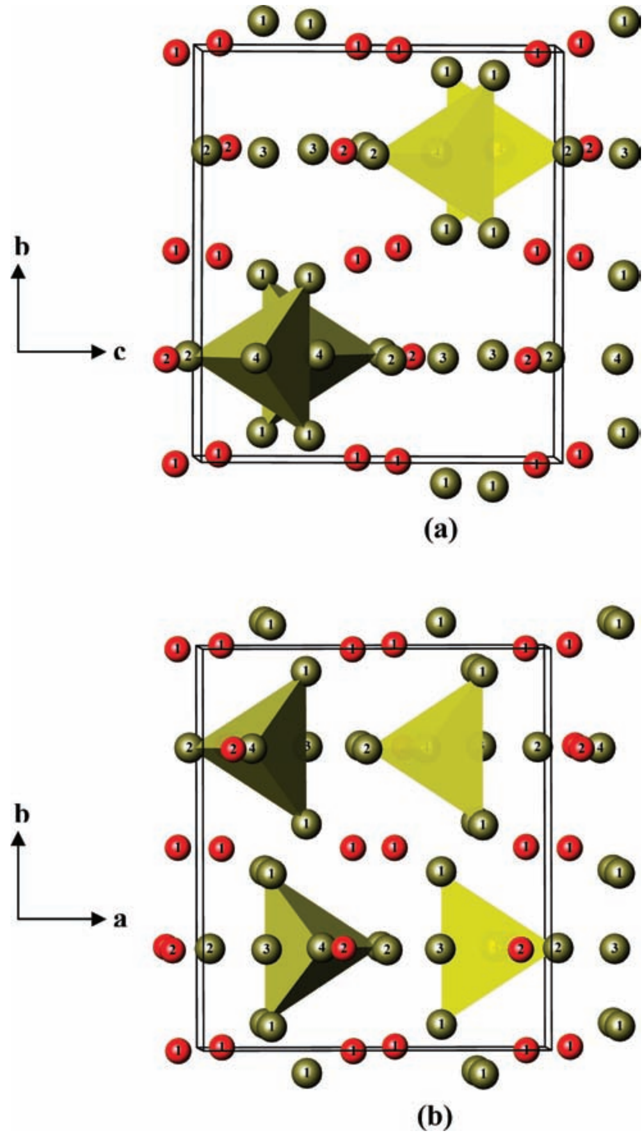

Figure 2. Projections of Er_5Sb_3 or Tm_5Sb_3 as (a) β-Yb_5Sb_3-type (*Y*) and (b) Y_5Bi_3-type (*YB*) structures onto [100] and [001], respectively, with the metal tetrahedra described in the text highlighted. Chains of tetrahedral cavities are evident only in the *Y*-type structure, a reasonable basis for the binding of H, *F* therein (yellow/olive figures are at different depths).

interstitial derivative utilizing the less regular tetrahedra in the *YB*-type structure has been recognized.

A number of questions remains about the parallel chemistry of 5−3 antimonides and bismuthides of the normally trivalent rare-earth metals with respect to their occurrence in some of these three structure types and their sensitivities to interstitial hydrogen. Antimonides in the group of R = Y,[9] Gd−Ho along with Gd_5Bi_3 and Tb_5Bi_3[10] reportedly exhibit hexagonal *M*-type structures near room temperature. The two bismuthides transform to orthorhombic *YB*-type structures at higher temperatures,[11] the remaining bismuthides for *Y*[3] and Dy−Er[12] being reported only in the latter type structure. However, some exceptions remain; three

(7) Hurng, W.-M.; Corbett, J. D. *Chem. Mater.* **1989**, *1*, 311.
(8) Franzen, H. F.; Khan, A. S.; Peterson, D. T. *J. Less-Common Met.* **1977**, *55*, 143.
(9) Schmidt, F. A.; McMasters, O. D. *J. Less-Common Met.* **1970**, *21*, 415.
(10) Rieger, W; Parthe, E. *Acta Crystallogr.* **1968**, *B24*, 456.
(11) Massalski, T. B. *Binary Alloy Phase Diagram*, 2nd ed.; The Materials Information Society, ASM International: Materials Park, OH, 1990.
(12) Oshihara, K.; Taylor, J. B.; Calvert, L. D.; Despault, J. G. *J. Less-Common Met.* **1975**, *41*, 329.

binaries have been reported with *Y*-type structures (an empty *F*-type), in contradistinction to the behavior of at least the divalent cation analogues, namely *Y*-types of Er_5Sb_3[13] and Sc_5Bi_3,[14] and of Sc_5Sb_3 in one case[15] but not in another.[16] Although no reports of impurity effects in these systems have appeared, these contradictory results naturally raised questions as to whether any of these examples may have contained unrecognized hydride or other impurities. Conversely, perhaps the electron-richer *Y*-type structures of trivalent cations may not require interstitials for stability.

We report here our results for stable R_5Sb_3 compounds, R = Y, Gd−Lu, over a range of compositions and temperatures with or without interstitials. Results include the discovery of new dimorphic orthorhombic examples (*YB*, *Y*) for Er_5Sb_3 and Tm_5Sb_3 and the refinement of all four structures from single crystal data. The corresponding R_5Bi_3 phases through Er were also examined with no significant deviations from literature data. The possible stabilization of orthorhombic R_5Pn_3 phases via nonstoichiometry or hydride or fluoride interstitials was also examined for the heavy lanthanides, with generally negative results.

Experimental Section

Syntheses. The starting materials were *Y*, Gd−Lu (Ames Laboratory, 99.95% total), Sb (Johnson Matthey, 99.9%, or Alfa-Aesar, 5-9's), and Bi pieces (Aldrich, 99.99%). All reactants and products were handled in glove boxes with 0.2−0.4 ppm H_2O levels. Exploratory reactions were generally carried out in sealed Ta containers heated either under dynamic vacuum or within evacuated, well-baked, and sealed silica jackets so as to eliminate (or greatly reduce) any hydrogen contamination from residual moisture. Arc-melting, wherever applicable, was conducted on a water-cooled Cu hearth within a glovebox and with a current of 30 A or less. Equimolar ratios of R:Sb were first heated in evacuated sealed silica tubes at 900 °C for 24 h.; then 3:2 molar proportions of this RSb and R were pelletized and arc-melted. (Arc-melting reactions for Tm systems were unsuitable owing to excessive evaporation.) All reactions above 1100 °C were done in a graphite-heated vacuum furnace (Thermal Technology Inc. model 1000A) under $<10^{-6}$ torr with samples sealed in Ta tubes under Ar and held in a Ta beaker which also acted as a getter. Quenching experiments were carried out with a $MoSi_2$-heated high temperature tube furnace (Thermolyne 54500). Samples in Ta/SiO_2 containers heated under argon were quenched by quickly pushing these out of the alumina core into cold water and immediately breaking the silica jacket, about a 5 s process.

All products were analyzed at ambient temperatures with the aid of Guinier X-ray powder patterns secured from Enraf-Nonius FR552 (film) or Huber 670 Guinier (image-plate) cameras with Cu $K\alpha_1$ radiation (λ= 1.540598 Å). All products are visually stable in air at room temperature for months. Yield distributions on a volume percent basis were estimated from the powder pattern of products relative to those calculated according to single crystal refinements. The close similarity of *Y* and *YB* polytypes means that yield estimates are mole percent values as well. Lattice constants were refined from the powder pattern data using the *UnitCell* program.[17]

Single crystals were picked from crushed samples and, as an initial precaution, mounted in glass capillaries. Those of low temperature forms were obtained from a stoichiometric Er_5Sb_3 reaction at 1400 °C for 4 h followed by cooling at 10 °C/h to 650 °C, or of Tm_5Sb_3 after a comparable reaction at 1300 °C for 10 h followed by cooling to 600 at 8 °C/h, both then being radiatively cooled to room temperature. Crystals of *Y*-Tm_5Sb_3, the (supposed) higher temperature form, were obtained from a mixed product after this composition had been reacted at 1250 °C for 72 h and further cooled to room temperature at 100 °C/h. Single crystals of Lu_5Sb_3 were obtained after annealing an arc-melted button in Ta at 1200 °C for 12 h in the vacuum furnace.

Structure Determination. Single crystal diffraction data from *YB*-type Er_5Sb_3 and Tm_5Sb_3 were collected on a Rigaku AFC6R diffractometer with monochromated Mo Kα radiation. Data were collected for the orthorhombic cell determined from a least-squares refinement of the setting angles of 25 indexed reflections. Systematic absences for $h + k = 2n + 1$ and $l = 2n + 1$ in the $hk0$ and $h0l$ zones, respectively, suggested space groups $Pc2_1n$ and *Pcmn*. The standard setting of the latter, *Pnma,* was selected for the structure solution, and the structure was subsequently refined successfully starting with positional data for the *YB* prototype Y_5Bi_3.[3] The isotropic refinement converged to residuals (R/R_w) of 11 and 13%. The final anisotropic refinement led to the residuals of 3.4/4.1%.The uneventful refinement of *YB*-Tm_5Sb_3 proceeded similarly and converged with R/R_w = 2.3/3.0%.

Diffraction data for *Y*-Tm_5Sb_3 and *YB*-Lu_5Sb_3 were secured on a Bruker SMART APEX CCD diffractometer equipped with graphite-monochromatized Mo Kα radiation in the form of 1800 frames for each with an acquisition time of 10 s per frame. Data were corrected for absorption and Lorentz polarization with *SADABS*.[18] Structure determinations and refinements were performed with the *SHELXTL*[19] program. The space group *Pnma* was assigned on the basis of the *mmm* Laue symmetry, the systematic absences, and the mean $|E^2 - 1|$ values. For *Y*-Tm_5Sb_3, all atomic positions were located by direct methods and refined anisotropically by full-matrix least-squares on F^2. The refinement converged with R_1 = 2.41%, wR_2 = 6.09% for $I > 2\sigma(I)$ data and 2.52 and 6.12% for all data, respectively., The isotropic refinement of Lu_5Sb_3 converged quickly with the atomic coordinates of *YB*-Er_5Sb_3, and the anisotropic refinement converged with R_1 = 2.18%, wR_2 = 4.28% for $I > 2\sigma(I)$ data and 2.64 and 4.44%, respectively, for all data.

Some crystallographic and refinement data for all four structures are listed in Table 1. The corresponding atomic coordinates, standardized with *STRUCTURE TIDY*,[20] and the isotropic-equivalent displacement parameters are listed in Table 2 for the two Tm_5Sb_3 phases and in Table S2, Supporting Information, for *Y*-types Er_5Sb_3 and Lu_5Sb_3. Distances in the last pair are also in the Supporting Information, Table S3. Tables of more refinement data and anisotropic displacement parameters for all structures are provided in the Supporting Information as well as the CIF's for the last two studies. (F_o/F_c data from the Rigaku studies are available on request.)

Magnetic Susceptibilities. Data for the *YB*-Er_5Sb_3 and *YB*-Tm_5Sb_3 were measured at 3 T over a range of 6−300 K with a Quantum Design (MPMS) SQUID magnetometer. The weighed

(13) Borzone, G.; Fornasini, M. L. *Acta Crystallogr.* **1990**, *C46*, 2456.
(14) Haase, M. G.; Block, H.; Jeitschko, W. *Z. Anorg. Allg. Chem.* **2001**, *627*, 1941.
(15) Berger, R. *Acta Chem. Scand.* **1977**, *A31*, 514.
(16) Maggard, P. A.; Knight, D. A.; Corbett, J. D. *J. Alloys Compd.* **2001**, *315*, 108.
(17) Holland, T. J. B.; Redfern, S. A. T. *Mineral. Mag.* **1997**, *61*, 65.
(18) Blessing, R. H. *Acta Crystallogr.* **1995**, *A51*, 33.
(19) *SHELXTL*; Bruker AXS, Inc.: Madison, WI, 2000.
(20) Gelato, L. M.; Parthe′, E. J. *J. Appl. Crystallogr.* **1987**, *20*, 139.

Table 1. Some Crystal Data and Refinement Parameters for *YB*-Er_5Sb_3, *Y*- and *YB*-Tm_5Sb_3, and *YB*-Lu_5Sb_3

	Er_5Sb_3 (*YB*)	Tm_5Sb_3 (*YB*)	Tm_5Sb_3 (*Y*)	Lu_5Sb_3 (*YB*)
formula weight	1201.55	1209.90		1240.10
crystal system		orthorhombic		
space group, *Z*		*Pnma*, 4		
		cell dimensions, Å		
a	7.9646(9)	7.9262(5)	11.6034(5)	7.8847(4)
b	9.176(1)	9.1375(6)	9.1077(4)	9.0770(5)
c	11.662(1)	11.6013(7)	7.9841(4)	11.5055(6)
volume, Å^3	852.2(3)	840.2(1)	843.76(7)	823.44(8)
ρ (cal), g/cm^3	9.363	9.564	9.524	10.003
data/res/param	1115/0/44	1105/0/44	1086/0/44	1064/0/44
GoF on F^2	1.488	1.187	1.385	1.092
R_1, wR_2 [$I > 2\sigma(I)$]	0.034, 0.041	0.023, 0.030	0.0241, 0.0609	0.0218, 0.0428
R_1, wR_2 (all data)			0.0252, 0.0612	0.0264, 0.0444

Table 2. Atomic Coordinates[a] and Isotropic-Equivalent Displacement Parameters (Å^2 × 10^3) for the Tm_5Sb_3 Structures

	x	*y*	*z*	*U*(eq)[b]
		YB-Tm_5Sb_3		
Tm1	0.1948(1)	0.0598(1)	0.0606(1)	12(1)
Tm2	0.0286(1)	1/4	0.5093(1)	9(1)
Tm3	0.1860(1)	1/4	0.7798(1)	14(1)
Tm4	0.3544(1)	1/4	0.2864(1)	17(1)
Sb1	0.0660(1)	0.0029(1)	0.3265(1)	13(1)
Sb2	0.4129(2)	1/4	0.5409(1)	10(1)
		Y-Tm_5Sb_3		
Tm1	0.0664(1)	0.0584(1)	0.1908(1)	8(1)
Tm2	0.0047(1)	1/4	0.5251(1)	7(1)
Tm3	0.2284(1)	1/4	0.8248(1)	10(1)
Tm4	0.2914(1)	1/4	0.3435(1)	9(1)
Sb1	0.3255(1)	0.0093(1)	0.0639(1)	8(1)
Sb2	0.4766(1)	1/4	0.5960(2)	8(1)

[a] 8d Wyckoff site for R1 and Sb1, 4c for other atoms. [b] *U*(eq) is defined as one-third of the trace of the orthogonalized U_{ij} tensor.

samples were held between two fused silica rods within a tightly fitting outer silica tube, and the assembly was sealed under helium, as before.[21] The raw data were corrected for the susceptibilities of the containers and the diamagnetic contributions of the atom cores.

Electronic Structure Calculations. Electronic structures for the *Y*- and *YB*-types of Tm_5Sb_3 were calculated self-consistently by the tight-binding linear muffin-tin-orbital (TB-LMTO) method[22−25] within the atomic sphere approximation (ASA) using the Stuttgart code.[26] Exchange and correlation were treated in a local spin density approximation (LSDA),[27] and scalar relativistic effects[28] were taken into account. The radii of Wigner−Seitz (WS) spheres were optimized according to an automatic procedure.[29] One empty sphere in an 8-fold general site was required for each. The WS radii so determined were 1.75−1.84 Å for Tm, 1.77−1.87 Å for Sb, and 1.11−1.20 Å for the empty sphere. The basis set included 6s, 6p, 5d, and 4f functions for Tm, 4s and 4p functions for Sb, and a 1s function for the empty spheres. The Tm 4f functions were treated as core orbitals containing 12 electrons. Reciprocal space integrations to determine self-consistent charge densities, density of states (DOS) curves, and crystal orbital Hamilton population (COHP)[30] analyses were performed by the tetrahedron method[31] using 112 *k*-points in the irreducible wedges of the corresponding Brillouin zones.

Total electronic energies of the two forms of Tm_5Sb_3 as well as a potentially intermediate structure were calculated as a function of volume using the Vienna ab initio simulation package (VASP).[32−34] All calculations were performed using projector augmented-wave (PAW) pseudopotentials[35] and the Perdew−Burke−Ernzerhof generalized gradient approximation (GGA-PBE).[36] A 7 × 7 × 7 Monkhorst−Pack *k*-points grid[37] was used to sample the first Brillouin zone for the reciprocal space integration. The energy cutoff of the plane wave basis was 215 eV. With these settings, the total energy converged to less than 1 meV per unit cell. At first, energy vs volume calculations were carried out for both the low-temperature and the high-temperature structures. The atomic positions were taken directly from the crystallographic data, and the volumes of the unit cells were varied isotropically. A set of "intermediate atomic positions" relative to the two standard types was established by averaging the atomic coordinates of the low-temperature and high-temperature structures in the standard setting of space group *Pnnm.* (For the lattice of the space group *Pnma*, the corresponding space group of the intermediate would be *Pnmn* along with a change of origin.) These atomic positions were then optimized within the unit cells of both structures.

Results and Discussion

Syntheses and Structure Type Distributions. Synthetic explorations among the binary R_5Sb_3 phases for R = Y, Gd−Ho confirmed the reported formation of hexagonal *M*-type structures with, in most cases, substantially the same lattice dimensions as reported in the literature, which came primarily from powder diffraction data. The same is true for *M*-type bismuthides of Gd[38,39] and *YB*-types for Y and Tb−Er. Reaction details, products, and lattice dimensions are given in Table 3 for one reaction for each compound and structure type, although more extensive investigations were completed.[40] Some reported unit cell volumes deviate from ours by up to ±0.7% (~5−7 Å^3), particularly for those from the older literature, but none of the differences suggest that substantial interstitial impurities had been involved earlier, in contrast to our experiences with divalent cations and hydrogen. A few $R_5(Sb,Bi)_3Z$ compositions were also investigated for *Z* = F or H, namely for $Y_5(Sb,Bi)_3F$, $Gd_5(Sb,Bi)_3(F,H)$, and $Er_5(Sb,Bi)_3F$, but in only one case did a meaningful change appear. This was the repeated appear-

(21) Guloy, A. M.; Corbett, J. D. *Inorg. Chem.* **1996**, *35*, 4669.
(22) Andersen, O. K. *Phys. Rev.* **1975**, *B12*, 3060.
(23) Andersen, O. K.; Jepsen, O. *Phys. Rev. Lett.* **1984**, *53*, 2571.
(24) Andersen, O. K.; Jepsen, O.; Glöotzel, D. In *Highlights of Condensed-Matter Theory*; Bassani, F., Fumi, F., Tosi, M. P., Lambrecht, W. R. L., Eds.; North-Holland: New York, 1985.
(25) Andersen, O. K. *Phys. Rev.* **1986**, *B34*, 2439.
(26) Tank, R.; Jepsen, O.; Burckhardt, H.; Anderson, O. K. *Program TB-LMTO 47*; Max-Plank-Institut für Festkörperforscchung: Stuttgart, Germany, 1994.
(27) von Barth, U.; Hedin, L. *J. Phys. C* **1972**, *5*, 1629.
(28) Koelling, D. D.; Harmon, B. N. *J. Phys. C* **1977**, *10*, 3107.
(29) Jepsen, O.; Andersen, O. K. *Z. Phys. B* **1995**, *97*, 645.
(30) Dronskowski, R.; Blöchl, P. *J. Phys. Chem.* **1993**, *97*, 8617.
(31) Blöchl, P. E.; Jepsen, O.; Andersen, O. K. *Phys. Rev.* **1994**, *B49*, 16223.
(32) (a) Kresse, G.; Hafner, J. *Phys. Rev. B* **1993**, *47*, 558. (b) Kresse, G.; Hafner, J. *Phys. Rev. B* **1994**, *49*, 14251.
(33) Kresse, G.; Furthmüller, *J. Comput. Mat. Sci.* **1996**, *6*, 15.
(34) Kresse, G.; Furthmüller, *J. Phys. Rev. B* **1996**, *54*, 11169.
(35) Kresse, G.; Joubert, D. *Phys. Rev.* **1999**, *59*, 1758.
(36) Perdew, J. P.; Burke, K.; Ernzerhof, M. *Phys. Rev. Lett.* **1996**, *77*, 3865.
(37) Monkhorst, H. J.; Pack, J. D. *Phys. Rev. B* **1976**, *13*, 5188.
(38) Hohnke, D.; Parthe, E. *J. Less-Common Met.* **1969**, *17*, 291.
(39) Holtzberg, F.; McGuire, T. R.; Methfessel, S.; Suits, J. C. *J. App. Phys.* **1964**, *35*, 1033.
(40) León-Escamilla, A. E. Ph.D. Dissertation, Iowa State University, 1996.

Table 3. R_5Pn_3 Phases for R = Y, Gd−Er and Pn = Sb, Bi: Reactions, Product Distributions, and Lattice Dimensions (∼293 K)

loaded comp	str types;[a] reaction types;[b] conditions[c]	*a* (Å)	*b* (Å)	*c* (Å)	*V* (Å³)	ref
Y_5Sb_3	M; AM	8.9114(5)		6.2960(6)	433.00(7)	9
Y_5Sb_3	Y: IF, *v*	11.867(1)	9.2247(9)	8.0977(8)	886.4(1)	34
Y_5Sb_3F	M; HTF *i*	8.9118(4)		6.2954(6)	433.00(6)	
Y_5Sb_3F	Y (M); HTF *ii*	11.869(1)	9.2317(8)	8.1034(7)	887.9(1)	
Y_5Bi_3	YB; AM	8.1895(4)	9.4202(4)	11.9753(6)	923.85(9)	3
Y_5Bi_3	YB; IF *iii*	8.201(1)	9.4296(8)	11.983(1)	926.7(2)	
Gd_5Sb_3	M; AM	8.975(4)		6.343(3)	442.5(2)	10
Gd_5Sb_3	M; HTF *i*	9.0173(3)		6.3242(3)	445.33(4)	
Gd_5Sb_3F	M (ATP); HTF *iv*	9.0252(7)		6.3239(5)	446.10(8)	
Gd_5Bi_3	M; AM	9.182(8)		6.426(7)	469.2(9)	38
Gd_5Bi_3	M; *sc*	9.1580(9)		6.4186(6)	466.20(9)	39
Gd_5Bi_3	M; HTF *iii*	9.1807(9)		6.406(1)	467.6(1)	
Gd_5Bi_3F	M; HTF *i*	9.1808(9)		6.4060(8)	467.6(1)	
Gd_5Bi_3	YB; IF *ii*	8.269(2)	9.550(2)	12.095(2)	955.1(4)	
$Gd_5Bi_3H_{4.5}$	YB (N); sc*iv*	8.248(2)	9.583(2)	12.090(4)	955.7(4)	
Tb_5Sb_3	M; AM	8.8.920(3)		6.304(3)	434.3(3)	10
Tb_5Bi_3	YB; *sc*	8.1993(8)	9.4759(9)	11.999(1)	932.3(1)	12
Tb_5Bi_3	YB; IF *iii*	8.1964(6)	9.4799(9)	11.9984(8)	932.3(1)	
Dy_5Sb_3	M; AM	8.870(4)		6.266(3)	427.0(4)	10
Dy_5Sb_3	M; HTF *i*	8.9023(5)		6.2577(5)	429.49(6)	
Dy_5Bi_3	YB; *sc*	8.1603(4)	9.4214(4)	11.9341(6)	917.5(1)	12
Dy_5Bi_3	YB; IF *iii*	8.1615(9)	9.4327(7)	11.9294(7)	918.4(1)	
Ho_5Sb_3	M; AM	8.851(2)		6.234(2)	422.9(2)	10
Ho_5Sb_3	M (N); HTF *i*	8.8573(3)		6.2277(4)	423.11(4)	
Ho_5Bi_3	YB; *sc*	8.1328(5)	9.3820(6)	11.8744(7)	906.0(1)	12
Ho_5Bi_3	YB; IF *iii*	8.130(1)	9.3812(9)	11.873(1)	905.5(2)	
Er_5Sb_3	Y; IF	11.662(1)	9.136(1)	8.007(1)	853.4(2)	13
Er_5Sb_3	Y; IF	11.6897(3)	9.1425(3)	8.0217(2)	857.3(1)	42
Er_5Sb_3	M; *sc*[d]	8.8062(4)		6.2139(4)	417.32(7)	42
Er_5Bi_3	YB; *sc*	8.0930(4)	9.3402(5)	11.8134(6)	892.98(9)	12
Er_5Bi_3	YB; IF *iii*	8.103(1)	9.3481(8)	11.810(1)	894.6(2)	
Tm_5Bi_3	YB; *sc*	8.0645(7)	9.3055(8)	11.758(2)	882.4(2)	12

[a] Structure types: *M* Mn_5Si_3-type (*P*6₃/*mcm*); *YB* low-temperature Y_5Bi_3-type (*Pnma*); *Y* high-temperature β-Yb_5Sb_3-type (*Pnma*); ATP anti-Th_3P_4; N NaCl, as discerned from Guinier powder patterns. [b] Reaction types: AM arc-melting; IF induction furnace. For samples sealed in Ta, HTF high temperature vacuum furnace; *sc* sealed SiO_2 jacket. [c] Reaction conditions: (*i*) 1400 °C for 4 h, to 650 °C at 10 °C/h, furnace off. (*ii*) 1400 °C for 2 h, to 1300 °C over l hr, anneal for 12 h, to RT at 18 °C/h. (*iii*) 1500 °C in IF for 1 h, 100 °C/h to 900 °C, furnace off. (*iv*) 1200 °C under high vacuum for 6 h, 10 °C/h to 650 °C. (*v*) 1400 °C, 8 h; radiatively cooled. [d] SiO_2 container only, 800 °C, 800 h.

ance of the *Y*-type $Y_5Sb_3F_x$ (mixed with normal *M*-type) after equilibrations for 12 h at 1300 °C followed by slow cooling, but not after 4 h at 1400 °C. Adequate single crystals for diffraction experiments could not be obtained. This result implies that some fluoride inclusion has increased the stability of the *Y*-type Y_5Sb_3 inasmuch as this binary phase has been isolated before only by means of radiative cooling from 1400 °C in an induction furnace, particular care being taken to exclude hydrogen from the system.[41] In contrast, cooling Er_5Sb_3F from 1200 °C led to a mixture of *YB*-type Er_5Sb_3 with insignificant deviations in lattice parameters plus unreacted ErF_3 and an unidentified Er-poorer phase.

Er_5Sb_3. One particular contrast among the results for the trivalent lanthanide pnictides originated with the 1990 report of the *Y*-type Er_5Sb_3 structure,[13] a type that we had earlier established was stable only with interstitial hydride or fluoride, at least among pnictides of the divalent lanthanide and alkaline-earth metals.[5−7] These Er_5Sb_3 crystals were obtained after presumed rapid cooling following fusion of the 5:3 composition (in a Ta container) through induction heating,[13] which occurred under high vacuum and made hydrogen contamination very unlikely. A more recent report concerns a *Y*-type Er_5Sb_3 phase (with a 0.4% larger cell volume, Table 3)[42] that was obtained by a different synthetic route, namely heating the questionable *M*-type compound (below) in Ta at 1250 °C for one week in an induction furnace followed by an unspecified cooling process. We have been unable to reproduce their *M*-type structure for low temperature Er_5Sb_3. Their hexagonal phase was obtained via equilibration of an arc-melted Er_5Sb_3 sample in SiO_2 (without a Ta container) at 800 °C for 800 h, circumstances that suggest possible contamination by H or O. The essential reversible formation of the hexagonal *M*-type structure from the high temperature *Y*-type was not demonstrated. Synthetic experiments designed to clarify these problems with Er_5Sb_3 as well as concomitant studies on the following Tm and Lu systems are listed in Table 4.

Further speculations that these diverse *Y*-Er_5Sb_3 results may have occurred via an unrecognized composition range for the phase or a fluoride impurity were ruled out experimentally. No *Y*-Er_5Sb_3 appeared following similar reactions of either $Er_5Sb_{3\pm x}$, or $Tm_5Sb_{3\pm x}$ (x = 0.5); thus only temperature appeared to be a significant thermodynamic variable for the *YB* → *Y* conversion. As detailed in Table 4, *Y*-Er_5Sb_3 was obtained in high yield single phase (>95 mol %), with very good dimensional agreement with the earlier report[13] as well, simply by arc-melting that composition, a method that should be closest to the earlier induction melting[13] as both cool relatively rapidly. Slower cooling of

(41) Mozharivskyj, Y.; Franzen, H. F. *J. Alloys Compd.* **2001**, *319*, 100.
(42) Zelinska, M.; Zhak, O.; Oryshchyn, S.; Babizhetskyy, V.; Pivan, J.-Y.; Guerin, R. *J. Alloys Compd.* **2007**, *437*, 133.

Table 4. Reaction Conditions, Products, and Lattice Constant Data for the 5:3 Antimonides of Er, Tm, and Lu

no.	loaded comp	reaction conditions	product and yield	*a* (Å)	*b* (Å)	*c* (Å)	vol (Å^3)
1	Er_5Sb_3	AM[a]	*Y* > 95%	11.6646(7)	9.1463(7)	8.0083(5)	854.40(7)
2	Er_5Sb_3	quench from 800 °C (24 h)	*YB* > 95%	7.9611(5)	9.1738(7)	11.6581(6)	851.43(7)
3	Er_5Sb_3	AM product from 2	*Y* > 95%	11.6633(6)	9.1449(6)	8.0072(5)	854.10(7)
4	Er_5Sb_3	1150 °C (12 h): Q[b]	*YB* ∼ 95%	7.9565(4)	9.1766(7)	11.6582(8)	851.21(7)
5	Er_5Sb_3	1200 °C (24 h): Q	*YB* ∼ 70% *Y* ∼ 30%				
6	Er_5Sb_3	1250 °C (72 h); Q	*YB* ∼ 50%, *Y* ∼ 50%				
7	Er_5Sb_3	1300 °C (12 h): Q	*Y* ∼ 95% *YB* ∼ 5%	11.661(1)	9.1497(8)	8.0077(6)	854.40(9)
8	Tm_5Sb_3	1400 °C (12 h) cool 100 °C/h[c]	*YB* ∼ 50%	7.9239(4)	9.1374(7)	11.5970(6)	839.67(6)
			Y ∼ 50%	11.601(1)	9.1050(7)	7.9840(6)	843.34(9)
9	Tm_5Sb_3	1400 °C (30 min.); Q	*Y* ∼ 90% *YB* ∼ 7%	11.6037(8)	9.1072(5)	7.9846(4)	843.80(5)
10	Tm_5Sb_3	1200 °C (12 h); Q	*Y* ∼ 80% *YB* ∼ 10%	11.602(1)	9.1043(7)	7.9821(7)	843.1(1)
11	Tm_5Sb_3	1050 °C (48 h); Q	*YB* ∼ 90% *Y* ∼ 5%	7.9262(5)	9.1375(8)	11.6013(7)	840.2(1)
12	Lu_5Sb_3	AM	*YB* + LuSb + U				
13	Lu_5Sb_3	1200 °C (12 h); Q	*YB* > 95%	7.8766(5)	9.0780(5)	11.5027(5)	823.49(5)

[a] Arc-melt (RSb + R), 20 A, 20 s each side. [b] Quenched reaction at indicated temperature. [c] High temperature vacuum furnace. *Y* β-Yb_5Sb_3-type, *YB* Y_5Bi_3-type (both *Pnma*); *U* unidentified phase.

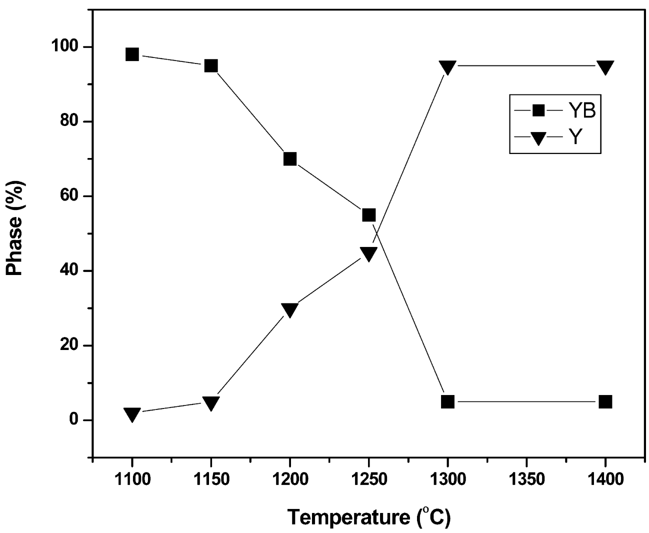

Figure 3. Variation of proportions of *Y*-type and *YB*-type Er_5Sb_3 products as a function of annealing temperature according to semiquantitative analyses of powder pattern results after quenching Er_5Sb_3 samples. The detection limits at the end points are 3−5 mol %.

other samples from 1300 or 1400 °C generally yielded the low temperature *YB*-Er_5Sb_3.

Quenching *Y*-Er_5Sb_3 samples from 800 °C yielded 95% *YB*-type (see the Experimental Section), and arc-melting the *YB* form to regain the *Y*-type established the reversibility of this transition (samples 1−3, Table 4). Well-baked silica jackets used in the first stage could still be a minor source of hydrogen, but the lattice constants were quite invariable. Further quenching experiments at first suggested that the transition took place over a range of temperatures. But, high yields of the low and high temperature *YB* and *Y* forms were obtained from samples quenched from the furnace temperatures of 1150 °C or below and 1300 °C or above, respectively. These and the intermediate phase distributions are plotted as a function of furnace temperatures in Figure 3 (samples 4−7, Table 4). Although the quenching rate is not extremely high, the transition is slow enough to gain mixtures of the polytypes from intermediate temperatures. These *Y*−*YB* mixtures cannot all represent equilibrium between the two Er_5Sb_3 phases. Rather, the residual *Y*-contents represent the fraction that remained when the quenching became particularly effective, probably close to the time the silica jacket was broken so that water made direct contact with the still red-hot Ta container (see the Experimental Section). A small amount of the *Y*-type (∼3−7 mol %) was present in the powder pattern of the sample quenched from 1150 °C, so the transition temperature must be lower. Its further definition was not pursued.

Tm_5Sb_3. The analogous Tm_5Sb_3 system is somewhat different synthetically and more challenging. Synthesis by arc-melting is not as useful because of the significant Tm volatilization that also occurs, giving about 70% of the *Y*-type but ∼30% TmSb (NaCl-type). (Comparative vapor pressure data suggest that Tm is closer to divalent as a liquid.[43]) Stoichiometric reactions targeting Tm_5Sb_3 in sealed Ta ampules in a vacuum furnace at 1300−1400 °C for 12 h followed by cooling at ∼100 °C/h yielded roughly equivolume mixtures of the *Y*- and *YB*-types. Slower cooling, 10 °C/h to 600 °C, or annealing at 800 °C for longer followed by quenching raised the *YB* yield to 70%. Again, quenched samples from 1400 or 1200 °C afforded mostly the *Y* form along with some TmSb. Furthermore, quenching the latter from 1050 °C led to about 90% *YB* form (Table 4, samples 9−12), putting the probable transition temperature somewhat below 1050 °C.

Lu_5Sb_3. The situation for Lu_5Sb_3 is unambiguous as syntheses by arc-melting, or by annealing either at 950 °C for 1 week or at 1200 °C for 12 h yielded only single phase *YB*-Lu_5Sb_3 samples. The reaction at 1200 °C also yielded single crystals suitable for diffraction analysis. Incidentally, the earlier assignment of a Lu_5Sb_3 composition found in a Lu−Sb phase diagram to the hexagonal *M*-type structure is unlikely, inasmuch as the rather imprecise hexagonal lattice constants reported ($a = 8.9$ Å, $c = 6.33$ Å) are, in fact, larger than those for *M*-Dy_5Sb_3[44] (Table 3). It is possible that contamination by adventitious interstitial impurities may have been responsible for the earlier observation.

(43) Gschneidner, K. A., Jr. *J. Less-Common Met.* **1971**, *25*, 405.
(44) Abdusalyamova, M. N.; Faslyeva, N. D.; Eliseev, A. A.; Shishkin, E. A.; Rakhmatov, O. I.; Chuiko, A. G.; Shumakova, T. P. *J. Less-Common Met.* **1990**, *166*, 229.
(45) Gschneidner, K. A., Jr. In *Handbook of Physics and Chemistry of Rare Earths, Cumulative Index*; Gschneidner, K. A., Jr., Eyring, L., Eds.; North-Holland Science Publishers B.V.: Amsterdam, 1993; Vol. 1−15, p 509.

Table 5. Selected Bond Distances in *YB*-Tm_5Sb_3 and *Y*-Tm_5Sb_3

YB-Tm_5Sb_3		*Y*-Tm_5Sb_3	
Tm1−Sb2	2.9656(7)	Tm1−Sb2	2.9515(1)
Sb2	3.066(1)	Sb2	3.0616(1)
Sb1	3.262(1)	Sb1	3.2045(1)
Tm2	3.2679(9)	Tm2	3.2678(1)
Sb1	3.290(1)	Sb1	3.2904(1)
Sb1	3.362(1)	Tm4	3.3687(1)
Tm4	3.3882(9)	Sb1	3.4418(1)
Tm1	3.476(1)	Tm1	3.4900(2)
Tm1	3.565(1)	Tm1	3.5760(1)
Tm2	3.6294(8)	Tm4	3.6470(1)
Tm4	3.666(1)	Tm2	3.7034(1)
Tm3	3.6928(8)	Tm3	3.8348(1)
Tm3	3.9209(8)	Tm3	3.8886(1)
Tm2−Sb2	3.067(2)	Tm2−Sb2	3.0433(2)
2Sb1	3.088(1)	2Sb1	3.0908(1)
2Sb1	3.112(1)	2Sb1	3.1043(1)
2Tm1	3.2679(9)	2Tm1	3.2678(1)
Tm3	3.377(1)	Tm3	3.4230(1)
2Tm1	3.6294(8)	Tm3	3.5302(1)
Tm4	3.654(1)	Tm4	3.6284(1)
Tm3	3.655(1)	2Tm1	3.7034(1)
Tm4	3.698(1)	Tm4	3.8455(1)
Tm3−Sb2	3.002(1)	Tm3−Sb2	2.9901(1)
2Sb1	3.082(1)	2Sb1	3.1177(1)
2Sb1	3.294(1)	2Sb1	3.2104(1)
Sb2	3.304(1)	Tm2	3.4230(1)
Tm2	3.377(1)	Sb2	3.4100(1)
Tm2	3.655(1)	Tm2	3.5302(1)
2Tm1	3.6928(8)	2Tm1	3.8348(1)
2Tm1	3.9209(8)	2Tm1	3.8886(1)
		Tm4	3.9117(2)
Tm4−Sb2	2.989(1)	Tm4−Sb2	2.9463(1)
2Sb1	3.103(1)	2Sb1	3.1538(1)
2Sb1	3.246(1)	2Sb1	3.2422(1)
2Tm1	3.3882(9)	2Tm1	3.3687(1)
Tm2	3.654(1)	Tm2	3.6284(1)
2Tm1	3.666(1)	2Tm1	3.6470(1)
Tm2	3.698(1)	Tm2	3.8455(1)
		Tm3	3.9117(2)

Magnetic Susceptibilities. The inverse magnetic susceptibilities of powdered samples of 95% *YB*-Er_5Sb_3 and Tm_5Sb_3 (plus traces of NaCl-type RSb) follow a Curie−Weiss relation over most of the (temperature range ($\theta = 0.3$ and 1.2 K, respectively), with the onset of some magnetic ordering below ~30−70 K. (Figure S2, Supporting Information)The effective magnetic moments, 22.28(1) and 16.90(2) $\mu_{B,}$ correspond to 9.96 and 7.56 μ_B per magnetic ion in Er_5Sb_3 and Tm_5Sb_3, which correspond fairly well to those associated with the trivalent cations, 9.58 and 7.56 μ_B for Er^{3+} and Tm^{3+}, respectively.[45]

Structures. The low-temperature *YB* and high-temperature *Y*-type structures are unambiguous in their assignments and in their differentiation (see Figure 1 and Tables 1 and 4), although the projections in Figure 1 suggest strong resemblances between the two types. The coordination environments surrounding each atom of the asymmetric units are very similar in both structure types: (a) there are no short Sb−Sb contacts; (b) Sb1 sites are surrounded by nine Tm atoms at less than 3.40 Å; (c) Sb2 sites are encapsulated by seven Tm atoms at distances less than about 3.40 Å; and (d) the metal atom environments around the Tm1 and Tm2 sites in the two structure types are very similar. The structural differences focus on the Tm3 and Tm4 sites: (a) these have one additional near-neighbor Tm atom in the high temperature *Y*-type structure than in the low temperature *YB*-type (the distance cutoff is set at 4.00 Å for this analysis) and (b) the 4-fold Tm3 and Tm4 sites become interchanged on comparing the *YB*- and *Y*-types.

The most striking features concerning the metal−metal contacts are the very short R1−R2 distances in all structures, 3.24−3.29 Å (depending on the intrinsic size of R), separations that are only about 0.1 Å greater than the Pauling's derived single bond lengths.[46] The shortest R−R distances of 3.29 and 3.27 Å in Er_5Sb_3 and Tm_5Sb_3, respectively (Table S3, Supporting Information and Table 5), strongly suggest trivalent states for the cations as do magnetic data for the *YB* forms of both (above). Strong bonding among the rare-earth elements in these phases is a natural attribute of these metal-rich structures, and six to eight R neighbors are found below 4 Å in all cases (see Table 5), with the average R−R distances in both *Y*- and *YB*-type structures being very similar. Simple electron counting provides a strong indicator for such metal−metal bonding: with no short Sb−Sb contacts, each Sb may be formulated as closed shell "Sb^{3-}", and R_5Sb_3 will have six valence electrons per formula unit left for R−R bonding. To accommodate these valence electrons, both the low-temperature *YB* and high-temperature *Y* forms feature metal tetrahedra that are built from two R1, one R2, and one R4 sites, as highlighted in Figure 2 for Er_5Sb_3 (examples are also dotted red in Figure 1). Each tetrahedron is similarly surrounded by Sb atoms; five Sb atoms bridge edges and two Sb atoms cap faces. The *subtle* differences occur with two additional *metal* atom neighbors: one each of R3 and R4, which bridge edges or cap open faces of the tetrahedra, i.e., those not capped by Sb atoms. (The two assemblies are detailed in Figure S3, Supporting Information.) *The R−R distances in this group in the ambient temperature YB form are 3−5% shorter than in the Y form.* This subtlety has a profound effect on the electronic density of states for the two structure types.

Electronic Structures. TB-LMTO-ASA calculations were carried out for the refined (room temperature) *Y*- and *YB*-type Tm_5Sb_3 structures in order to understand their bonding characteristics. The corresponding densities of states (DOS) and the relevant crystal orbital Hamilton population (COHP) curves for *YB*-Tm_5Sb_3 and the quenched high-temperature *Y* form are depicted in Figures 4 and 5, respectively. The DOS curves for both structure types have similarities: (i) a narrow band attributed to Sb 5s wave functions lies around 10 eV below the Fermi level (E_F); (ii) a narrow energy gap between the Sb 5p-based valence band and largely Tm (5d, 6s)-based conduction band occurs ca. 1.6 eV below E_F; and (iii) pseudogaps exist at the Fermi levels. The inset in each shows an expanded view of the DOS around E_F, which make these pseudogaps clearer. Particularly noteworthy is the "deeper" pseudogap present in the DOS curve of the *YB* structure type as compared with that of the *Y*-type. The tightly bound metal tetrahedra in both structures account for the pseudogaps; the subtle differences in how Tm3 and Tm4 cap these tetrahedra lead to the qualitatively different features of these pseudogaps. The stronger Tm−Tm overlaps present

(46) Pauling, L. *The Nature of the Chemical Bond*, 3rd ed.; Cornell University Press: Ithaca, NY, 1960; p 403.

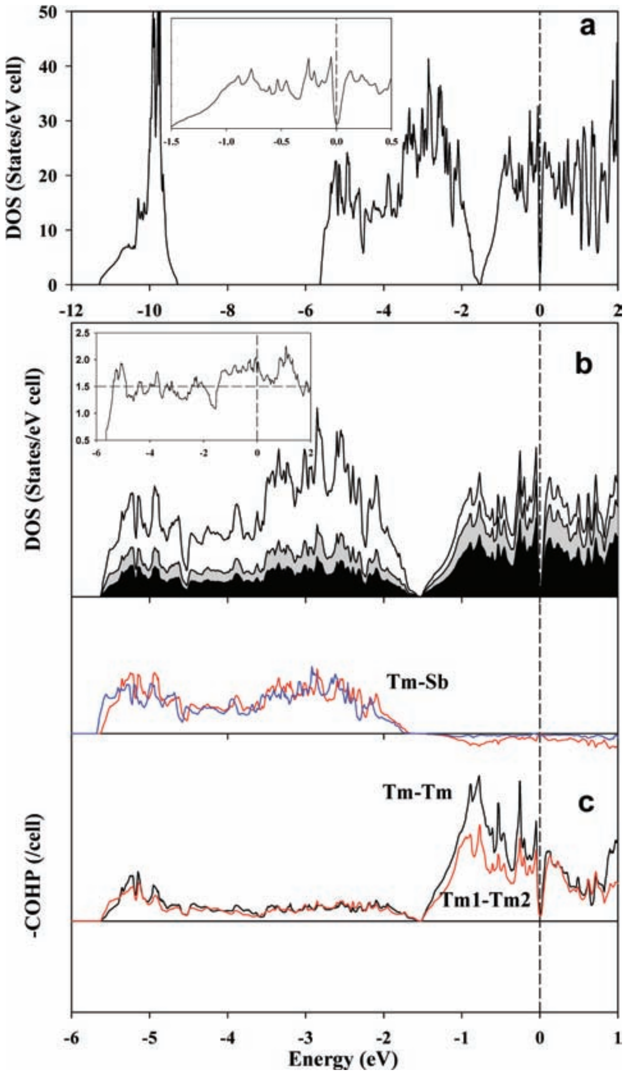

Figure 4. (a) Total DOS plot for the low-temperature *YB*-Tm_5Sb_3. The inset shows an expanded view in the region of E_F. (b) Stacked PDOS of Tm1 + Tm2 (black), Tm3 + Tm4 (gray), and Sb (white) for *YB*-Tm_5Sb_3. The inset shows the ratio of (Tm1+ Tm2)/(Tm3+ Tm4) partial DOS. (c) −COHP data for *YB*-Tm_5Sb_3. (top section) Tm−Sb1 (blue); Tm−Sb2 (red). (bottom) Average Tm1−Tm2 (black), average Tm−Tm (red). Dashed lines correspond to the Fermi energy.

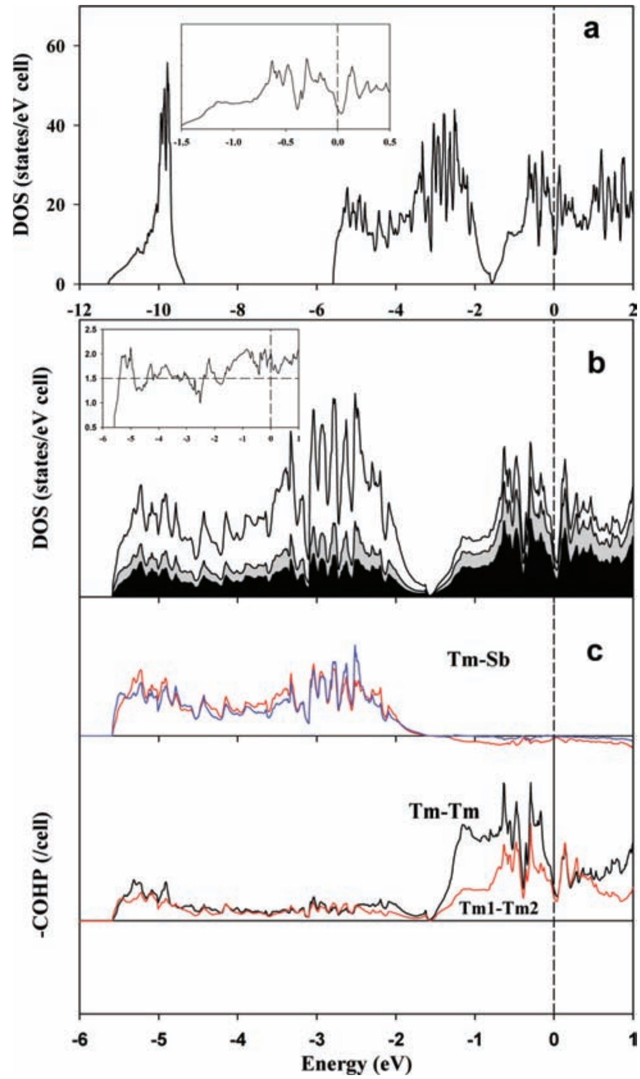

Figure 5. (a) Total DOS data for the high temperature *Y*-Tm_5Sb_3. The inset shows an expanded view in the region of E_F. (b) Stacked PDOS of Tm1 + Tm2 (black), Tm3 + Tm4 (gray), and Sb (white) for *Y*-Tm_5Sb_3. The inset shows the ratio of (Tm1+ Tm2)/(Tm3+ Tm4) partial DOS. (c) −COHP data for *Y*-Tm_5Sb_3. (top section) Tm−Sb1 (blue); Tm−Sb2 (red). (bottom) Average Tm1−Tm2 (black), average Tm−Tm (red). Dashed lines correspond to the Fermi energy.

in the low-temperature *YB*-type lead to a clearer separation in the electronic states of the tetrahedron, with six Tm-based (5d, 6s) states dropping below E_F. Figures 4b and 5b show stacked partial DOS projections of (Tm1 + Tm2) (black), (Tm3 + Tm4) (gray), and Sb (white), which make clear the larger involvement of Tm1 and Tm2 5d orbitals, including in the definition of the pseudogap, in the *YB* form. Insets to Figures 4b and 5b show the ratios of DOS for (Tm1 + Tm2)/DOS of (Tm3 + Tm4). These average close to the relative number of atoms involved (12/8 = 1.5) over the lower valence band (below ca. −1.6 eV), but they clearly become dominated by Tm1 + Tm2 states in the conduction band. −COHP data in Figures 4c and 5c demonstrate that there is little difference between Sb1 and Sb2 in bonding to Tm (top sections), but that the average −COHP values for all Tm1−Tm2 interactions in the conduction band (black curves) are clearly greater than the average for all Tm−Tm bonds (bottom). The latter effects are also notably less in the high temperature form. Greater reduction of Tm1 and Tm2 is indicated, in line with their shorter separations.

To investigate the transition between the low-temperature *YB* form and the high-temperature *Y* form, VASP pseudopotential calculations were carried out on both structures of Tm_5Sb_3, as well as for a hypothetical intermediate structure constructed to represent the transition from one type to the other. (NOTE: this structural intermediate is not meant to imply a mechanism but simply to explore an "average" of the *YB* and *Y* forms.) This intermediate structure adopts the space group *Pnmn* (standard setting is *Pnnm*) following the similarities shown in Figure 1 (see Table S5, Supporting Information, for its parameters). In this setting, the low-temperature *YB* form adopts the space group *Pnma*, whereas the high-temperature *Y* form takes the space group *Pcmn*.

The results of VASP calculations at common unit cell volumes indicate $E(YB) < E(Y)$, in agreement with fact. Both

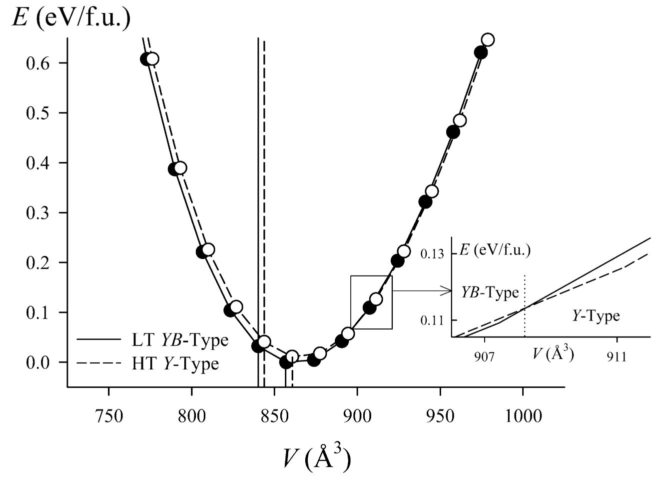

Figure 6. Comparison of energy vs volume curves for Er_5Sb_3 as the *YB* (solid line) and the *Y* (dashed) structures as calculated on the basis of their room temperature structures.

are significantly lower in energy (by ca. 0.9 eV/formula unit) than the intermediate case. A comparison of energy vs volume curves, Figure 6, further indicates that the *Y*-type achieves a lower total energy than the *YB*-type at higher unit cell volumes, although this effect does not occur at the minimum energy. The comparison made as a function of volume thus mimics thermal expansion, not the effects of heating. (At room temperature, the experimental cell volume of *Y* is 3.6 Å^3 (0.4%) greater than that for *YB*.) Structural optimization efforts using VASP reveal that both *YB* and *Y* forms are local minima on the total energy surface, but there is no experimental evidence that the hypothetical intermediate structure actually forms. In fact, this model is *not a local minimum* on the total energy surface, but consistently optimizes toward the *YB*-type. Evaluation of the energy bands for the intermediate structure shows additional degeneracies in the wave functions at certain Brillouin zone boundary points, degeneracies that are broken for both the *YB*- and *Y*-type structures (Figures S4 and S5, Supporting Information) in a manner similar to a Peierls distortion. It is important to emphasize, however, that the transition between the *YB*- and *Y*-type structures does not meet the criteria for a symmetry-breaking ("second-order") phase transition, but a thorough characterization of the nature of this transition in the solid-state has not been investigated.

Other Reports of *Y*-type Structures for These Compounds. The results of this study make it clear that Er_5Sb_3 and Tm_5Sb_3 are the *only* R_5Pn_3 phases, Pn = Sb or Bi, for which a β-Yb_5Sb_3-type (*Y*) structure clearly exists. However, the factors differentiating the two obvious choices appear to be too complex in detail for the present results to be generalized to include metals with different valence electron counts or elements of materially different sizes, e.g., Ti and As.[47]

There are some other phases, however, for which uncertain or contradictory classifications in this structural group remain. Sc_5Sb_3 was first stated to adopt a *Y*-type structure according to powder diffraction data from its mixture with ScSb that had been prepared by arc-melting and further reaction in sealed fused silica at 950 °C.[15] (Hydrogen problems in these structures were not known at that time.) On the other hand, the *YB* structure was later assigned to Sc_5Sb_3 according to Guinier data from a single phase sample that had been slowly cooled from 1100 °C or above in a high temperature vacuum furnace.[16] On the other hand, hydrogen (or other) impurities seem unlikely considering the care and experimental conditions employed in the study of *Y*-Sc_5Bi_3,[14,48] so the difference is possibly because of the marked change in the size of R (above). No ternary hydrides or fluorides appear to form with *YB*-type structures either, consistent with the *YB* versus *Y* structure (Figure 2) as well as earlier studies of 5−3 pnictides of divalent cations. The situation with the recently reported hydrogen-free *Y*-type Yb_5Bi_3 by Liang et al.[49] deserves mention. Their synthesis of this included a potential source of H or O (Ta/SiO_2 containers), and although one H analysis was said to show no such impurity, their cell dimensions are well within those obtained earlier for $Yb_5Bi_3H_x$ systems containing moderate to low hydrogen contents.[5] More importantly, the formation of the known hexagonal Mn_5Si_3-polytype for binary Yb_5Bi_3 was not observed, a phase that can be obtained only under very low hydrogen concentrations as afforded by quenching samples from 1100 °C in high vacuum.[2] Furthermore, their cell volumes do show a decrease with increased hydrogen content, contrary to their statement.

Finally, we know this *Y* structure type with two extremes of chemistry and bonding among the rare-earth-metal pnictides. The present two antimonide examples with trivalent R feature strong R−R bonding in a metal- and electron-rich environment in which delocalized bonding appears dominant. At the other extreme are the so-called isotypic "salts" R_5Pn_3Z, stuffed *Y*-type examples in which R is a nominal divalent example (Sm, Eu, Yb) or an alkaline-earth metal Ca−Ba, and Z is, to date, H or F.[5] These are, in contrast, nominal Zintl (valence) compounds in which electron localization is predominant. Still the same R_4 tetrahedra are features at both extremes; the Zintl phase structures well-refined for both Ca_5Sb_3F[7] and Ca_5Bi_3D[50] have interstitial atoms *Z* at the same centering positions as those defined by the tightly bound Tm_4 tetrahedra noted here. Why the latter do not also form hydrides or fluorides is a more complicated question.

Conclusions

Four new phases, Y_5Bi_3-type Er_5Sb_3, β-Yb_5Sb_3 and Y_5Bi_3-types of Tm_5Sb_3, and Y_5Bi_3-type Lu_5Sb_3 are obtained in high yields under controlled synthetic conditions. Thus far, Er_5Sb_3, Tm_5Sb_3, and Lu_5Sb_3 are the only examples of trivalent rare-earth metal R_5Sb_3 phases that crystallize in a *YB*-type structure. Furthermore, the heavier erbium and thulium members are the only ones among trivalent rare-earth pnictides that transform to the *Y* type at higher temperatures (1000−1200 °C). All other R_5Sb_3 compounds of these

(47) Lee, C.-S.; Dashjav, E.; Kleinke, H. *J. Alloys Compd.* **2002**, *338*, 60.
(48) Jeitschko, W., private communication.
(49) Liang, Y.; Gil, R. C.; Schnelle, W.; Schmidt, M.; Zhao, J. T.; Grin, Y. *Z. Naturforsch.* **2007**, *62b*, 935.
(50) León-Escamilla, A. E.; Dervenagas, P.; Stassis C.; Corbett, J. D. unpublished research.

elements (Gd−Ho) phases crystallize in the hexagonal *M*-type structure. Experiments spanning broad compositional and reaction conditions have disproved the involvement of interstitials in any of these transformations. R_5Bi_3 (R = Gd−Tm) phases crystallize in *YB*-type structure with the exception of Gd_5Bi_3 and Tb_5Bi_3, the latter two transforming to the *M*-type structure at low temperatures. Theoretical results for both forms of Tm_5Sb_3 emphasize the major influence of Tm−Tm bonding, the separation of Sb-dominated valence band from a Tm-based conduction band and, in the *YB* form, the presence of a deep pseudogap at E_F and stronger Tm−Tm bonding.

Acknowledgment. Professor W. Jeitschko provided significant information regarding the synthesis of Sc_5Bi_3. We thank J. Ostenson for the magnetic susceptibility measurements. This research was supported by the office of the Basic Energy Sciences, Materials Sciences Division, U.S. Department of Energy; the Ames Laboratory is operated for the DOE by Iowa State University under contract no. W-7405-Eng-82.

Supporting Information Available: Comparison of simulated powder patterns of *Y*- and *YB*-Er_5Sb_3, magnetic susceptibility plots for *YB*-Er_5Sb_3 and *YB*-Tm_5Sb_3, details of the augmented Tm_4 cluster structures in the twoTm_5Sb_3 phases, electronic energy bands for *Y*-Tm_5Sb_3, *YB*-Tm_5Sb_3, and the hypothetical intermediate structure, listings of crystallographic data and the anisotropic displacement parameters for *Y*-Tm_5Sb_3, *Y*- and *YB*-Er_5Sb_3, and *YB*-Lu_5Sb_3, CIF outputs for the last two, and crystallographic coordinates of a hypothetical intermediate structure for Tm_5Sb_3. This material is available free of charge via the Internet at http://pubs.acs.org.

IC802464U